# Steel 8615 CA Axial Sim. Carb. Core-Geom. Test Iteration #155

## Monotonic Tensile and Fatigue Test Results

Prepared by:

Yikai Yin

and

Hong-Tae Kang

Department of Mechanical Engineering
College of Engineering and Computer Science
The University of Michigan-Dearborn
Dearborn, Michigan 48128

Prepared for:
The AISI Bar Steel Applications Group

April 2014

American Iron and Steel Institute
2000 Town Center, Suite 320
Southfield, Michigan 48075
tel: 248-945-4777
fax: 248-352-1740
www.autosteel.org

# TABLE OF CONTENTS

# NOMENCLATURE

| | | | |
|---|---|---|---|
| $A_o$, $A_f$ | initial, final area | S | engineering stress |
| HB, HRB, HRC | Brinell, Rockwell B-Scale, Rockwell C-Scale Hardness Number | YS, UYS, LYS, YS′ | monotonic yield, upper yield, lower yield, cyclic yield strength |
| b, c, n | fatigue strength, fatigue ductility, strain hardening exponent | YPE | yield point elongation |
| $D_o$, $D_f$ | initial, final diameter | $S_u$ | ultimate tensile strength |
| e | engineering strain | EL% | percent elongation |
| E, E′ | monotonic, cyclic strength coefficient | RA% | percent reduction in area |
| K, K′ | monotonic, cyclic strength coefficient | $\sigma$, $\sigma_f$, $\sigma_f'$ | true stress, true fracture strength, fatigue strength coefficient |
| $L_o$, $L_f$ | initial, final gage length | $\varepsilon_e$, $\varepsilon_p$, $\varepsilon$ | true elastic, plastic, total strain |
| $N_{50\%}$, $(N_f)_{10\%}$, $(N_f)_{50\%}$ | number of cycles to midlife, 10% load drop, 50% load drop | $\varepsilon_f$, $\varepsilon_f'$ | true fracture ductility, fatigue ductility coefficient |
| $P_f$, $P_u$ | fracture, ultimate load | $\varepsilon_a$, $\varepsilon_m$, $\Delta\varepsilon$ | strain amplitude, mean strain, strain range |
| R | strain ratio | $\Delta\varepsilon_e$, $\Delta\varepsilon_p$ | elastic, plastic strain range |

# UNIT CONVERSION TABLE

| Measure | SI Unit | US Unit | From SI to US | From US to SI |
|---|---|---|---|---|
| Length | mm | in | 1 mm = 0.03937 in | 1 in = 25.4 mm |
| Area | $mm^2$ | $in^2$ | 1 $mm^2$ = 0.00155 $in^2$ | 1 $in^2$ = 645.16 $mm^2$ |
| Load | kN | klb | 1kN = 0.2248 klb | 1 klb = 4.448 kN |
| Stress | MPa | ksi | 1 MPa = 0.14503 | 1 ksi = 6.895 MPa |
| Temperature | $^oC$ | $^oF$ | $^oC$ = ($^oF$ - 32) /1.8 | $^oF$ = ($^oC$ * 1.8) + 32 |

In SI Unit

1 kN = $10^3$ N  1 Pa = 1 $N/m^2$  1 MPa = $10^6$ Pa = 1 $N/mm^2$  1 GPa = $10^9$ Pa

In US Unit

1 klb = $10^3$ lb  1 psi = 1 $lb/in^2$  1 ksi = $10^3$ psi

# SUMMARY

Monotonic tensile properties and fatigue behavior data were obtained for steel material of iteration 155. The material was provided by AISI. Two tensile tests were performed to acquire the desired monotonic properties. Both tests gave similar results. Fourteen constant amplitude strain-controlled fatigue tests at seven strain levels were performed to obtain the fatigue life and cyclic deformation curves and properties. The experimental procedure followed and results obtained are presented and discussed in this report.

# I. EXPERIMENTAL PROGRAM

## 1.1 Material and Specimen Fabrication

### 1.1.1 Material

The steel material was provided by AISI. The test specimen was prepared from an 8615 CA Axial steel grade with the condition of simulated carburized core. Inclusion distribution and microstructure of the material are shown in Figure 1 and 2, respectively. The hardness of this material is 97 HRB or 20 HRC (see Appendix B).

### 1.1.2 Specimen

In this study, identical round specimens were used for monotonic and fatigue tests. The specimen configuration and dimensions are shown in Figure 3. This configuration deviates slightly from the specimens recommended by ASTM Standard E606 [1]. The recommended specimens have uniform gage sections. The specimen geometry shown in Figure 3 differs by using a large secondary radius in the gage section to compensate for the slight stress concentration at the gage to grip section transition.

All specimens were provided by Chrysler. Heat treatment and Machining were needed at first. The specimens were then polished prior to testing by a local polishing company (McNichols Polishing & Anodizing Inc.) near the University of Michigan-Dearborn. All remaining polishing marks coincided with the longitudinal direction of the specimen. The polished surfaces were carefully examined under magnification to ensure complete removal of the machine marks within the test section. Test specimens were protected immediately after machining and polishing until they were tested, since they may be susceptible to corrosion in moist room-temperature air.

Before testing, the measurement of each specimen was needed. The measured dimensions are shown in Table A.3. Imprint specimen numbers on both ends of the test section in regions of low stress, away from grip contact surfaces.

## 1.2 Testing Equipment

### 1.2.1 Apparatus

A MTS 810 Material Test System which included a closed-loop sevro-controlled hydraulic axial load frame was used to conduct both monotonic and fatigue tests. The load cell used had a capacity of 100 kN. The MTS 646 Hydraulic Collet Grips with 0.50 in (12.7mm) diameter collets were employed to secure the specimens' ends in series with the load cell.

Total strain was controlled and measured using an extensometer rated as ASTM class B1 [2]. Here in this study, MTS Model 632.26E-20 Extensometer was chosen. The calibration of the extensometer was verified by the professional of the MTS. The extensometer had a gage length of 0.30 in and was capable of measuring strains up to 15%.

In order to protect the specimens' surface from the knife-edges of the extensometer, ASTM Standard E606 recommends the use of transparent tape or epoxy to 'cushion' the attachment. For this study, it was found that the application of transparent tape strips was difficult due to the size of the test section. Therefore, epoxy was considered to be the best protection. The tests were performed using M-coat A. Prior to the testing, made marks on both side of each specimen's gage length where the knife-edges of the extensometer can be set up. After each specimen was broken, observe the failure location and see if it is inside the gage length.

### 1.2.2 Alignment

Alignment of the load path components was essential for the accurate measurement of strain-life material constants. Significant effort was put forth to align the load path components (such as load cell, grips, specimens, and actuator). Misalignment can result from both tilt and offset between the central line of the load train components. The alignment was done by the professional of the MTS in accordance with ASTM Standard E1012 [3].

## 1.3 Test Methods and Procedures

### 1.3.1 Monotonic tension tests

Monotonic tests in this study were performed using test methods specified by ASTM Standard E8 [4]. Two specimens were used to obtain the monotonic properties.

In order to protect the extensometer, strain control was used up to 10% strain, until the point of ultimate tensile strength had been crossed. After this point, displacement control was used until fracture. MTS 793.00 System Software and MTS 793.10 MultiPurpose Testware were used for the monotonic tests. The specimens are tested to fracture under strain or displacement control. For the elastic and initial yield region (0% to 0.5% strain) as well as the period up to which the extensometer was removed, a strain rate of 0.0025 in/in/min (0.001 mm/mm/s) was chosen. This strain rate was three-quarters of the maximum allowable rate specified by ASTM Standard E8 for the initial yield region. After the extensometer was removed, a displacement rate of 0.006 in/min (0.00254 mm/s) was used.

After the tension tests were concluded, the broken specimens were carefully reassembled. The final gage lengths of the fractured specimens, the final diameter, and the necking radius were then measured by a digital caliper for several times to make sure that the results were accurate. It should be noted that prior to the test, the initial diameter was measured with this same instrument.

### 1.3.2 Constant amplitude fatigue tests

Constant-amplitude axial fatigue tests provide information about the cyclic and fatigue behavior of materials. All constant amplitude fatigue tests in this study were performed according to ASTM Standard E606. It is recommended by this standard that at least 10 specimens by used to generate the fatigue properties. For this study, 14 specimens at 7 different strain amplitudes ranging from 0.2% to 2.000% were utilized. MTS 793.00 System Software and MTS 793.10 MultiPurpose Testware were used in all strain-controlled tests. During each strain-controlled test, the total strain was recorded using the extensometer output. Test data were automatically recorded

throughout each test.

There were two control modes used for these tests. Strain control was used in all tests with plastic deformation. For one of the elastic tests, strain control was used initially to determine the stabilized load, then load control was used for the reminder of the test and for the rest of the elastic tests, load control was used throughout. One reason for the change in control mode was due to the frequency limitation on the extensometer. Besides, at long lives, the total strain becomes quite small and the control of these quantities requires accurate instrumentation and extreme precision in the test procedure. Tests with anticipated lives exceeding 1 million cycles are change to load control mode when the load are stabilized. For the strain-controlled test, the applied frequencies ranged from 0.2 Hz to 5.0Hz in order to keep a strain rate about 0.02 in/in/sec. For the load-controlled tests, load waveforms with frequencies of up to 25Hz were used in order to shorten the overall test duration. All tests were conducted using a triangular waveform except the tests run at 25 Hz, when a sinusoidal waveform was used.

Failure of the specimens is defined when the maximum load decreases by 50% because of a crack or cracks being present. The strain-life curve is developed over a range of approximately 100 to 5,000,000 cycles (10,000,000 reversals).

# II. EXPERIMENTAL RESULTS AND ANALYSIS

## 2.1 Microstructural Data

A specimen was sectioned longitudinally from the grip end and transversely from the gage section to obtain a general microstructure description. The sample was prepared with standard test procedures for sectioning, mounting, polishing, and etched. The sample was reviewed and observed under a microscope. The microphotographs revealed the microstructure of the material. Figure 1 shows a low magnification photograph of the inclusion distribution in this kind of steel and Figure 2 shows a high magnification view of the microstructure from the gage area. Both of the figures were provided by Chrysler. The chemistry of the material is presented in Table 1.

## 2.2 Monotonic Deformation Behavior

The properties determined from monotonic tensile tests were the following: modulus of elasticity (E), yield strength (YS), ultimate tensile strength ($S_u$), percent elongation (%EL), percent reduction in area (%RA), true fracture strength ($\sigma_f$), true fracture ductility ($\varepsilon_f$), strength coefficient (K), and strain hardening exponent (n).

True stress ($\sigma$), true strain ($\varepsilon$), and true plastic strain ($\varepsilon_p$) were calculated from engineering stress (S) and engineering strain (e), according to the following relationships which are based on constant volume assumption:

$$\sigma = S(1 + e) \tag{1a}$$

$$\varepsilon = \ln(1 + e) \tag{1b}$$

$$\varepsilon_p = \varepsilon - \varepsilon_e = \varepsilon - \frac{\sigma}{E} \tag{1c}$$

The true stress ($\sigma$) - true strain ($\varepsilon$) plot is often represented by the Ramberg -Osgood equation:

$$\varepsilon = \varepsilon_e + \varepsilon_p = \frac{\sigma}{E} + \left(\frac{\sigma}{K}\right)^{\frac{1}{n}} \tag{2}$$

The strength coefficient, K, and strain hardening exponent, n, are the intercept and slope of the best line fit to true stress (σ) versus true plastic strain ($\varepsilon_p$) data in log-log scale:

$$\sigma = K\left(\varepsilon_p\right)^n \tag{3}$$

In accordance with ASTM Standard E739 [5], when performing the least squares fit, the true plastic strain ($\varepsilon_p$) was the independent variable and the true stress (σ) was the dependent variable. These plots for the two tests conducted are shown in Figure 4. As can be seen from this figure, the two curves are very close to each other. To generate the K and n values, the range of data used in this figure was chosen according to the definition of discontinuous yielding specified in ASTM Standard E646 [6]. Therefore, the valid data range occurred between the end of yield point extension and the strain at maximum load.

The true fracture strength was corrected for necking according to the Bridgman correction factor [7]:

$$\sigma_f = \frac{\frac{P_f}{A_f}}{\left[1+\frac{4R}{D_f}\right]\ln\left[1+\frac{D_f}{4R}\right]} \tag{4}$$

where $P_f$ is load at fracture, R is the neck radius, and $D_f$ is the diameter at fracture.

The true fracture ductility, $\varepsilon_f$, was calculated from the relationship based on constant volume:

$$\varepsilon_f = \ln\left(\frac{A_0}{A_f}\right) = \ln\left(\frac{1}{1-RA}\right) \tag{5}$$

where $A_f$ is the cross-sectional area at fracture, $A_0$ is the original cross-sectional area, and RA is the reduction in area.

A summary of the monotonic properties for this material is provided in Table A.1. The monotonic stress-strain curves are shown in Figure 5. As can be seen from this figure, the two curves are very close to each other. Refer to Table A.1 for a summary of the monotonic test results.

## 2.3 Cyclic Deformation Behavior

### 2.3.1 Transient cyclic response

Transient cyclic response describes the process of cyclic-induced change in deformation resistance of a material. Data obtained from constant amplitude strain-controlled fatigue tests were used to determine this response. Plots of stress amplitude variation versus applied number of cycles can indicate the degree of transient cyclic softening/hardening. Also, these plots show when cyclic stabilization occurs. A composite plot of the transient cyclic response for the steel studied is shown in Figure A.1a, while a semi-log plot is shown in Figure A.1b. Even though multiple tests were conducted at each strain amplitude, data from one test at each strain amplitude tested are shown in these plots.

### 2.3.2 Steady-state cyclic deformation

Another cyclic behavior of interest was the steady state or stable response. Data obtained from constant amplitude strain-controlled fatigue tests were also used to determine this response. The properties determined from the steady-state hysteresis loops were the following: cyclic modulus of elasticity (E′), cyclic strength coefficient (K′), cyclic strain hardening exponent (n′), and cyclic yield strength (YS′). Half-life (midlife) hysteresis loops and data were used to obtain the stable cyclic properties.

Similar to monotonic behavior, the cyclic true stress-strain behavior can be characterized by Ramberg-Osgood type equation:

$$\frac{\Delta\varepsilon}{2} = \frac{\Delta\varepsilon_e}{2} + \frac{\Delta\varepsilon_p}{2} = \frac{\Delta\sigma}{2E} + \left(\frac{\Delta\sigma}{2K'}\right)^{\frac{1}{n'}} \quad (6)$$

It should be noted that in Equation 6 and the other equations that follow, E is the average modulus of elasticity that was calculated from the monotonic tests.

The cyclic strength coefficient, K′, and cyclic strain hardening exponent, n′, are the intercept and slope of the best line fit to true stress amplitude ($\Delta\sigma/2$) versus true plastic strain amplitude ($\Delta\varepsilon_p/2$) data in log-log scale:

$$\frac{\Delta\sigma}{2} = K'\left(\frac{\Delta\varepsilon_p}{2}\right)^{n'} \quad (7)$$

In accordance with ASTM Standard E739 [5], when performing the least squares fit, the true plastic strain amplitude ($\Delta\varepsilon_p/2$) was the independent variable and the stress amplitude ($\Delta\sigma/2$) was the dependent variable. The true plastic strain amplitude was calculated by the following equation:

$$\frac{\Delta\varepsilon_p}{2} = \frac{\Delta\varepsilon}{2} - \frac{\Delta\sigma}{2E} \quad (8)$$

This plot is shown in Figure 6. To generate the K′ and n′ values, the range of data used in this figure was chosen for $\left[\frac{\Delta\varepsilon_p}{2}\right]_{calculated} \geq 0.001$ in/in.

The cyclic stress-strain curve reflects the resistance of a material to cyclic deformation and can be vastly different from the monotonic stress-strain curve. The cyclic stress-strain curve is shown in Figure 7. In Figure 8, superimposed plots of monotonic and cyclic curves are shown. As can be seen in this figure, the material cyclically softened. Figure A.2 shows a composite plot of the steady-state (midlife) hysteresis loops. Even though multiple tests were conducted at each strain amplitude, the stable loops from only one test at each strain amplitude are shown in this plot.

## 2.4 Constant Amplitude Fatigue Behavior

Constant amplitude strain-controlled fatigue tests were performed to determine the strain-life curve. The following equation relates the true strain amplitude to the fatigue life:

$$\frac{\Delta\varepsilon}{2} = \frac{\Delta\varepsilon_e}{2} + \frac{\Delta\varepsilon_p}{2} = \frac{\sigma_f'}{E}\left(2N_f\right)^b + \varepsilon_f'\left(2N_f\right)^c \quad (9)$$

where $\sigma_f'$ is the fatigue strength coefficient, b is the fatigue strength exponent, $\varepsilon_f'$ is the fatigue ductility coefficient, c is the fatigue ductility exponent, E is the monotonic modulus of elasticity, and $2N_f$ is the number of reversals to failure.

The fatigue strength coefficient, $\sigma_f'$, and fatigue strength exponent, b, are the intercept and slope of the best line fit to true stress amplitude ($\Delta\sigma/2$) versus reversals to failure ($2N_f$) data in log-log scale:

$$\frac{\Delta\sigma}{2} = \sigma_f'\left(2N_f\right)^b \tag{10}$$

In accordance with ASTM Standard E739 [5], when performing the least squares fit, the stress amplitude ($\Delta\sigma/2$) was the independent variable and the reversals to failure ($2N_f$) was the dependent variable. This plot is shown in Figure 9. To generate the $\sigma_f'$ and b values, all data, with the exception of the run-out tests, in the stress-life figure were used.

The fatigue ductility coefficient, $\varepsilon_f'$, and fatigue ductility exponent, c, are the intercept and slope of the best line fit to calculated true plastic strain amplitude ($\Delta\varepsilon_p/2$) versus reversals to failure ($2N_f$) data in log-log scale:

$$\left(\frac{\Delta\varepsilon_p}{2}\right)_{calculated} = \varepsilon_f'\left(2N_f\right)^c \tag{11}$$

In accordance with ASTM Standard E739 [5], when performing the least squares fit, the true plastic strain amplitude ($\Delta\varepsilon_p/2$) was the independent variable and the reversals to failure ($2N_f$) was the dependent variable. The calculated true plastic strain amplitude was determined from Equation 8. This plot is shown in Figure 10. To generate the $\varepsilon_f'$ and c values, the range of data used in this figure was chosen for $\left[\frac{\Delta\varepsilon_p}{2}\right]_{calculated} \geq 0.001$ in/in.

The true strain amplitude versus reversals to failure plot is shown in Figure 11. This plot displays the strain-life curve (Eqn. 9), the elastic strain portion (Eqn. 10), the plastic strain portion (Eqn. 11) and superimposed fatigue data. A summary of the cyclic properties for this steel is provided in Table 2. Table A.2 provides the summary of the fatigue test results.

A parameter often used to characterize fatigue behavior at stress concentrations, such as at the root of a notch, is Neuber parameter [7]. Neuber's stress range is given by:

$$\sqrt{(\Delta\varepsilon)(\Delta\sigma)E} = 2\sqrt{\left(\sigma_f'\right)^2\left(2N_f\right)^{2b} + \sigma_f'\varepsilon_f'E\left(2N_f\right)^{b+c}} \tag{12}$$

A plot of Neuber stress range versus reversals to failure is shown in Figure 12. This figure displays the Neuber curve based on Eqn. 12 and superimposed fatigue data for this material.

**Table 1: Chemical Composition of Steel 8615 (Courtesy of Chrysler)**

| Element | Wt.% |
|---|---|
| Carbon, C | 0.110% |
| Manganese, Mn | 0.840% |
| Phosphorus, P | 0.009% |
| Sulfur, S | 0.035% |
| Silicon, Si | 0.300% |
| Nickel, Ni | 0.400% |
| Chromium, Cr | 0.600% |
| Molybdenum, Mo | 0.200% |
| Copper, Cu | 0.140% |
| Tin, Sn | 0.007% |
| Aluminum, Al | 0.030% |
| Vanadium, V | 0.005% |
| Niobium, Nb | 0.002% |
| Oxygen, O | 0.0015% |

## Table 2: Summary of the Mechanical Properties

| Monotonic Properties | Average | Range |
|---|---|---|
| Modulus of elasticity, E, GPa: | 204.93 | 204.66 - 205.20 |
| Yield strength (0.2% offset), YS, MPa: | 753.2 | 750.1 – 756.2 |
| Ultimate strength, $S_u$, MPa: | 1011.0 | 1007.1 - 1014.8 |
| Percent elongation, %EL (%): | 36.5% | 36.2% - 36.7% |
| Percent reduction in area, %RA (%): | 61.5% | 61.0% - 61.9% |
| Strength coefficient, K, MPa: | 1516.3 | 1497.9 - 1534.7 |
| Strain hardening exponent, n: | 0.1091 | 0.1076 - 0.1106 |
| True fracture strength, $\sigma_f$, MPa: | 1438.3 | 1418.8 – 1457.9 |
| True fracture ductility, $\varepsilon_f$ (%): | 95.3% | 94.2% - 96.4% |
| **Cyclic Properties** | **Average** | **Range** |
| Cyclic modulus of elasticity, E′, GPa: | 200.66 | 194.3 – 206.6 |
| Fatigue strength coefficient, $\sigma_f'$, MPa: | 1545.4 | |
| Fatigue strength exponent, b: | -0.09 | |
| Fatigue ductility coefficient, $\varepsilon_f'$: | 1.6959 | |
| Fatigue ductility exponent, c: | -0.72 | |
| Cyclic strength coefficient, K′, MPa: | 1372.7 | |
| Cyclic strain hardening exponent, n′: | 0.116 | |
| Cyclic yield strength, YS′, MPa: | 580.6 | |
| Fatigue Limit (defined at $10^6$ cycles), MPa | 451.5 | |


Figure 1: Low magnification photograph of the inclusion distribution in the steel (Courtesy of Chrysler)

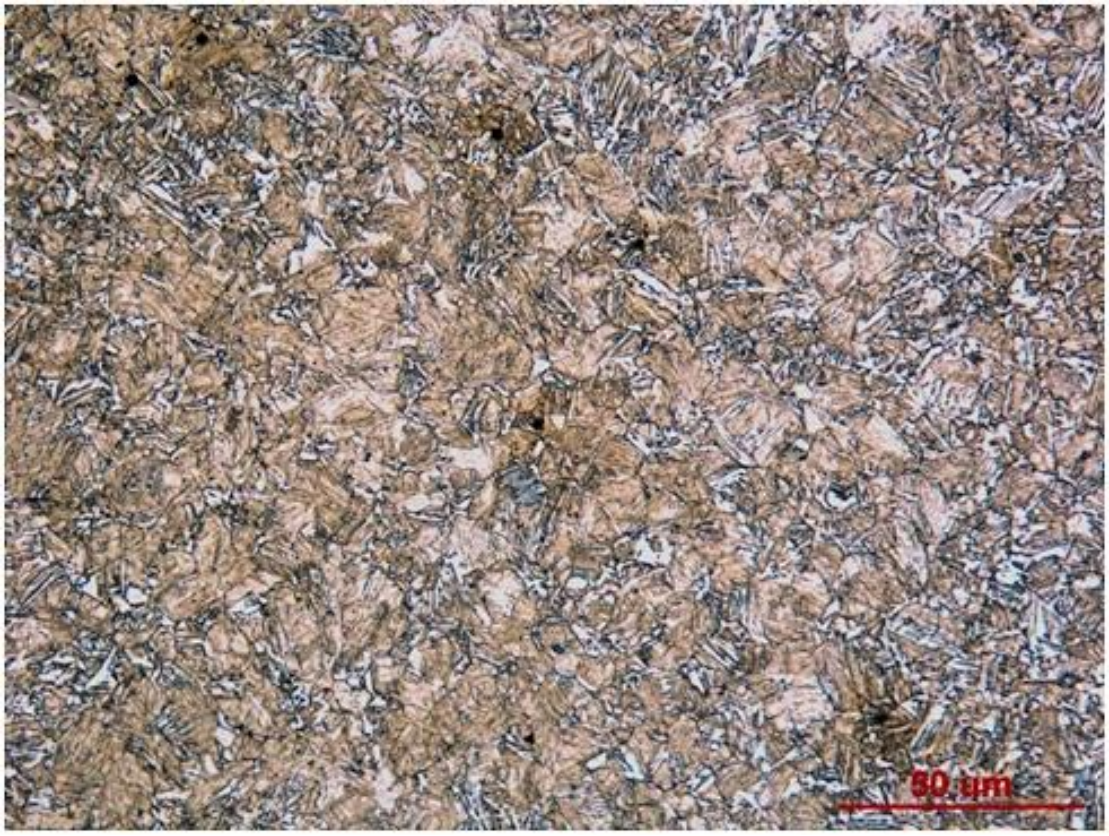


Figure 2: High magnification photo showing the microstructure of the transverse section from the gage area (Courtesy of Chrysler)

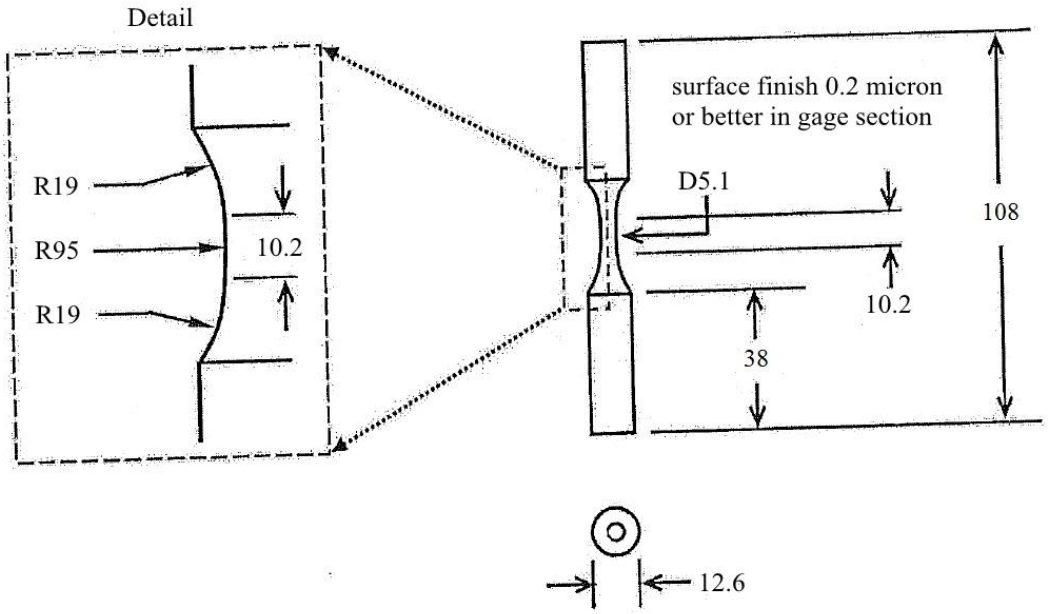


Figure 3: Specimen configuration and dimensions (mm)


Figure 4: True stress versus true plastic strain

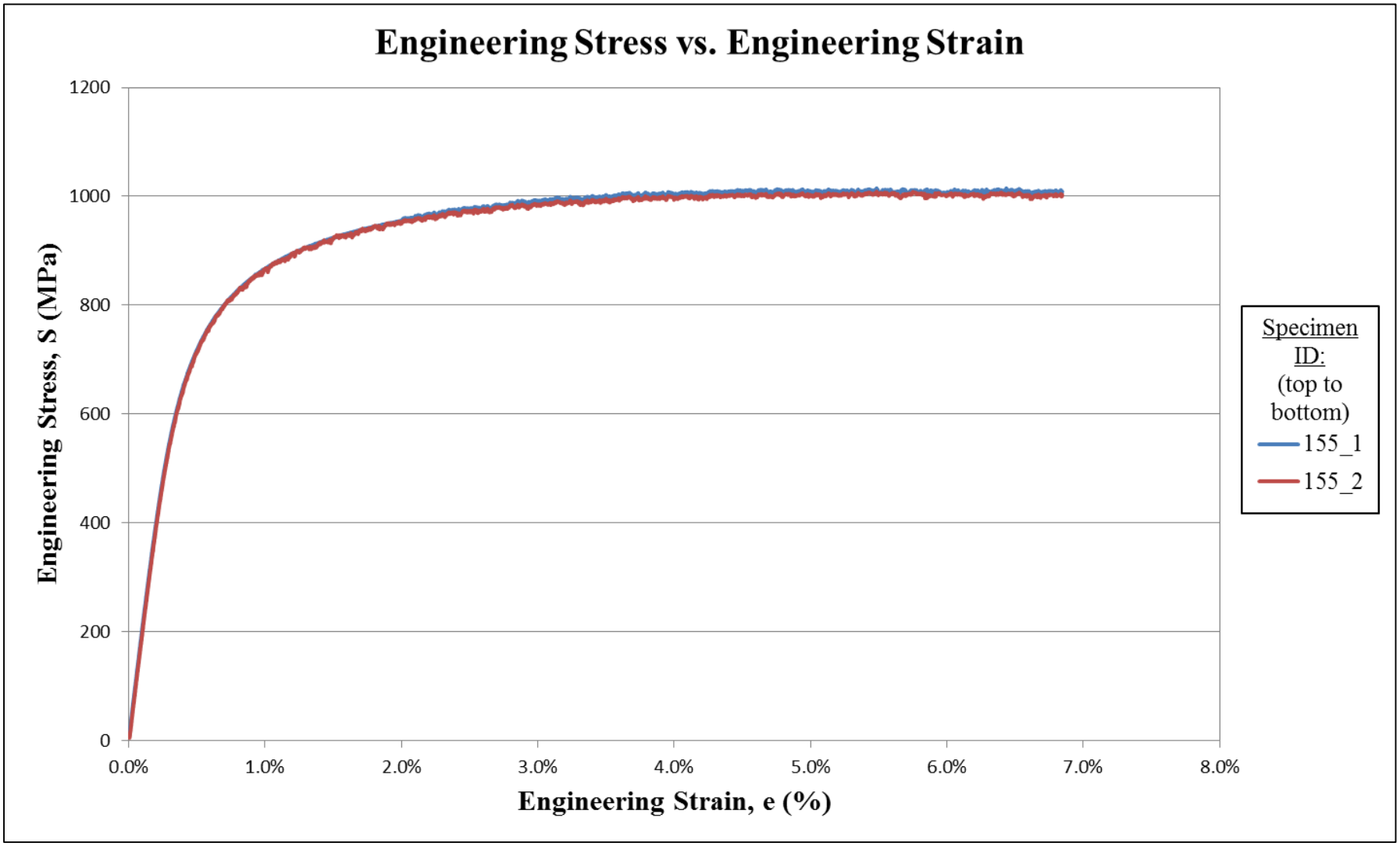


Figure 5: Monotonic stress-strain curves

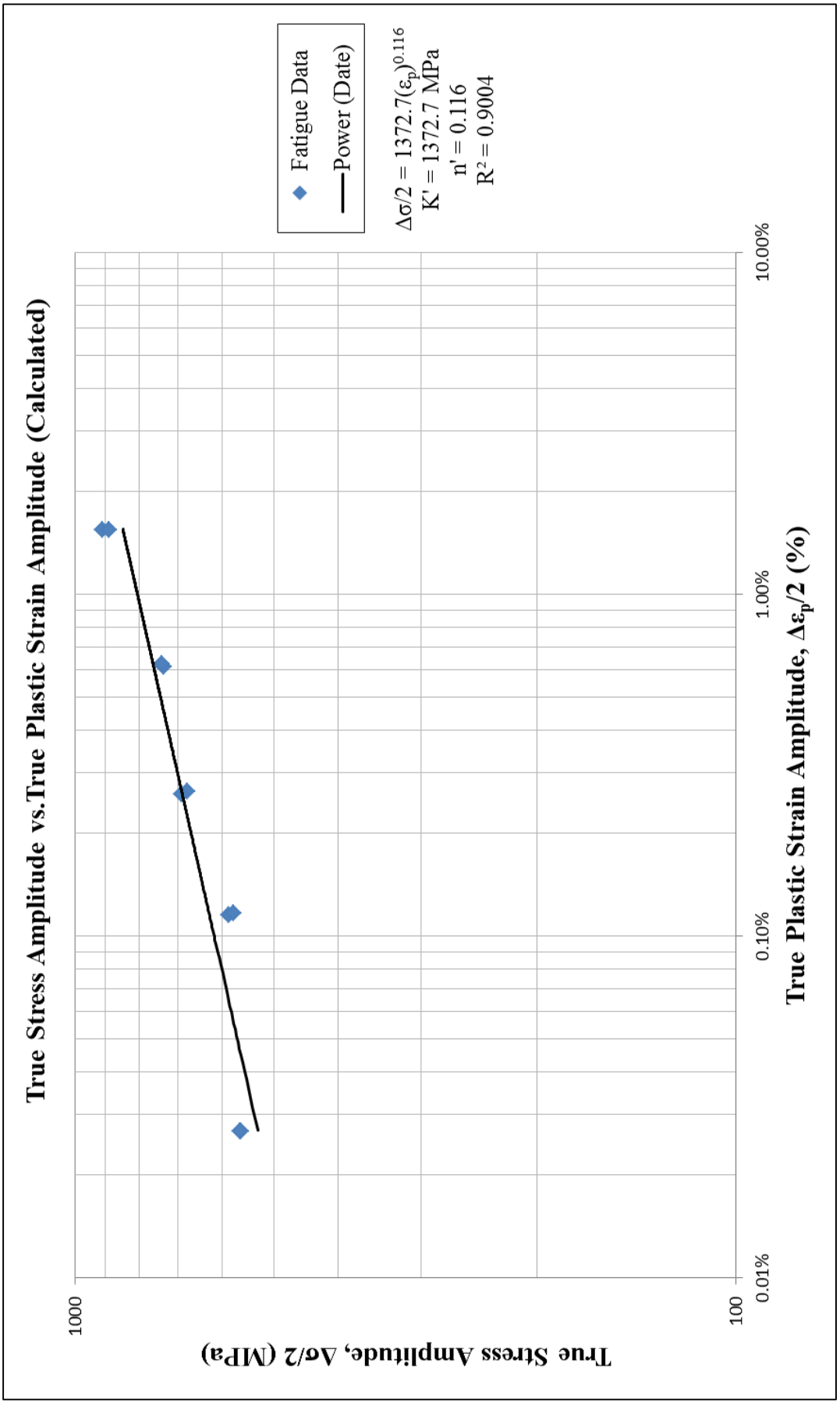


Figure 6: True stress amplitude versus true plastic strain amplitude (calculated)

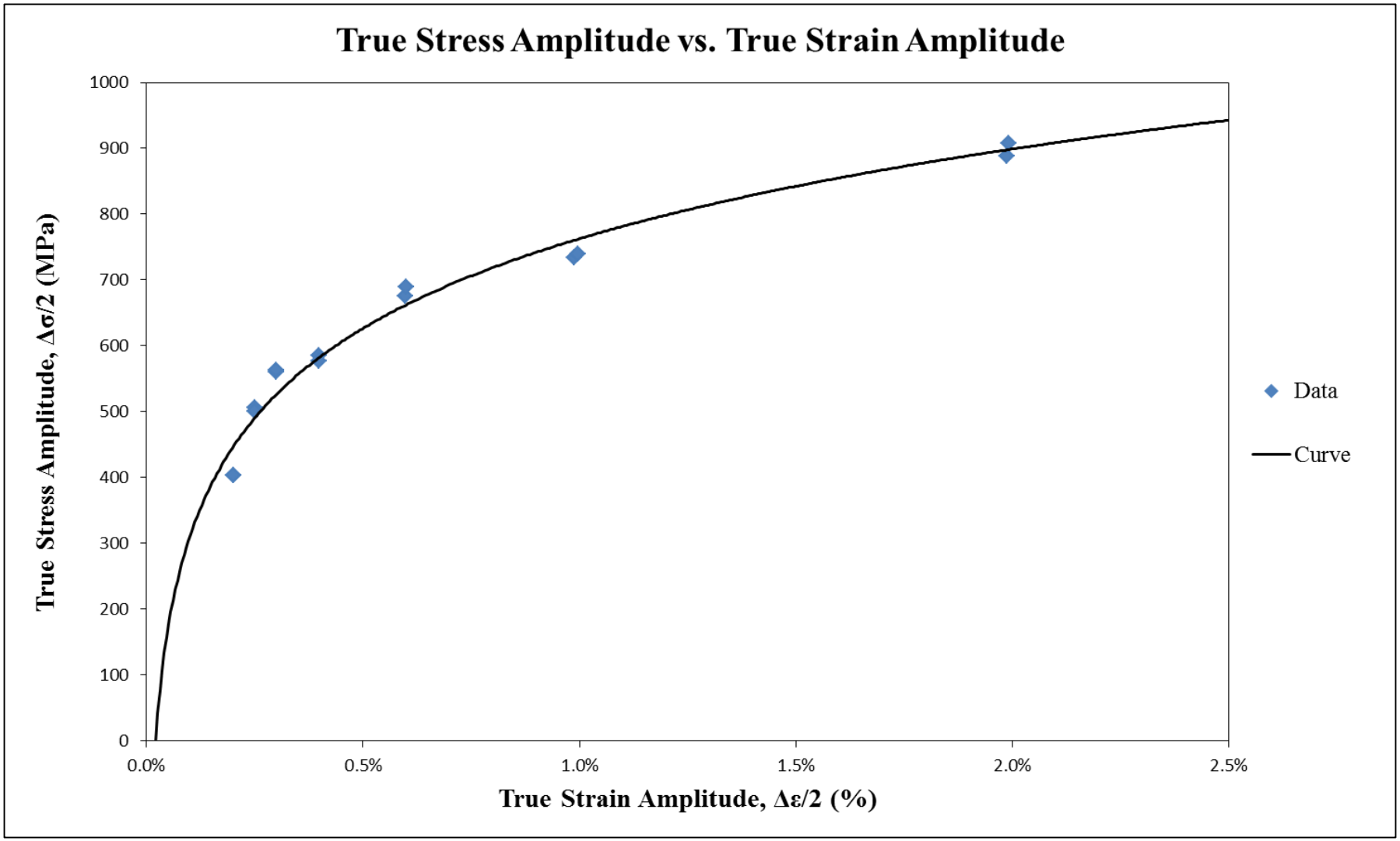


Figure 7: True stress amplitude versus true strain amplitude

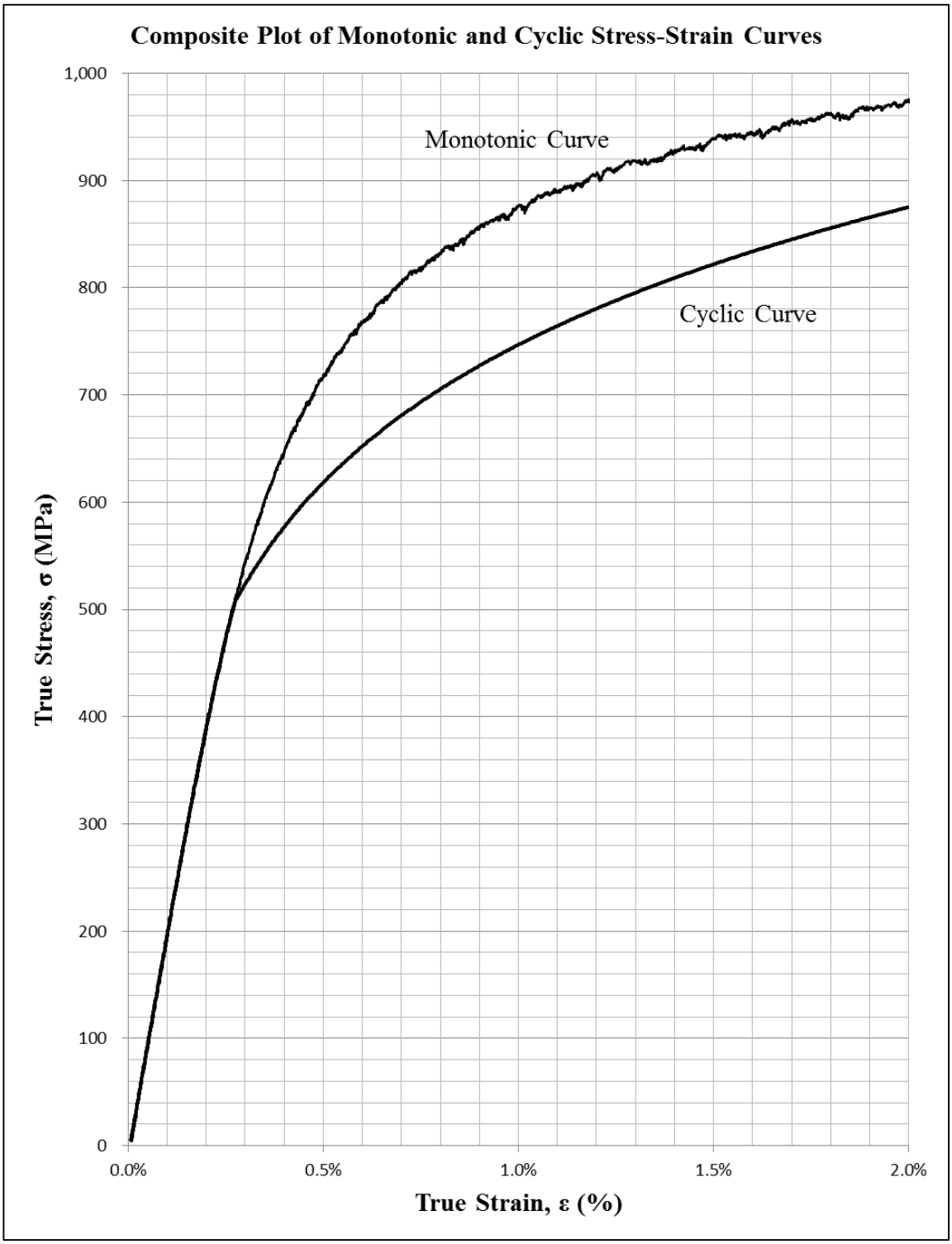


Figure 8: Composite plot of cyclic and monotonic stress-strain curves

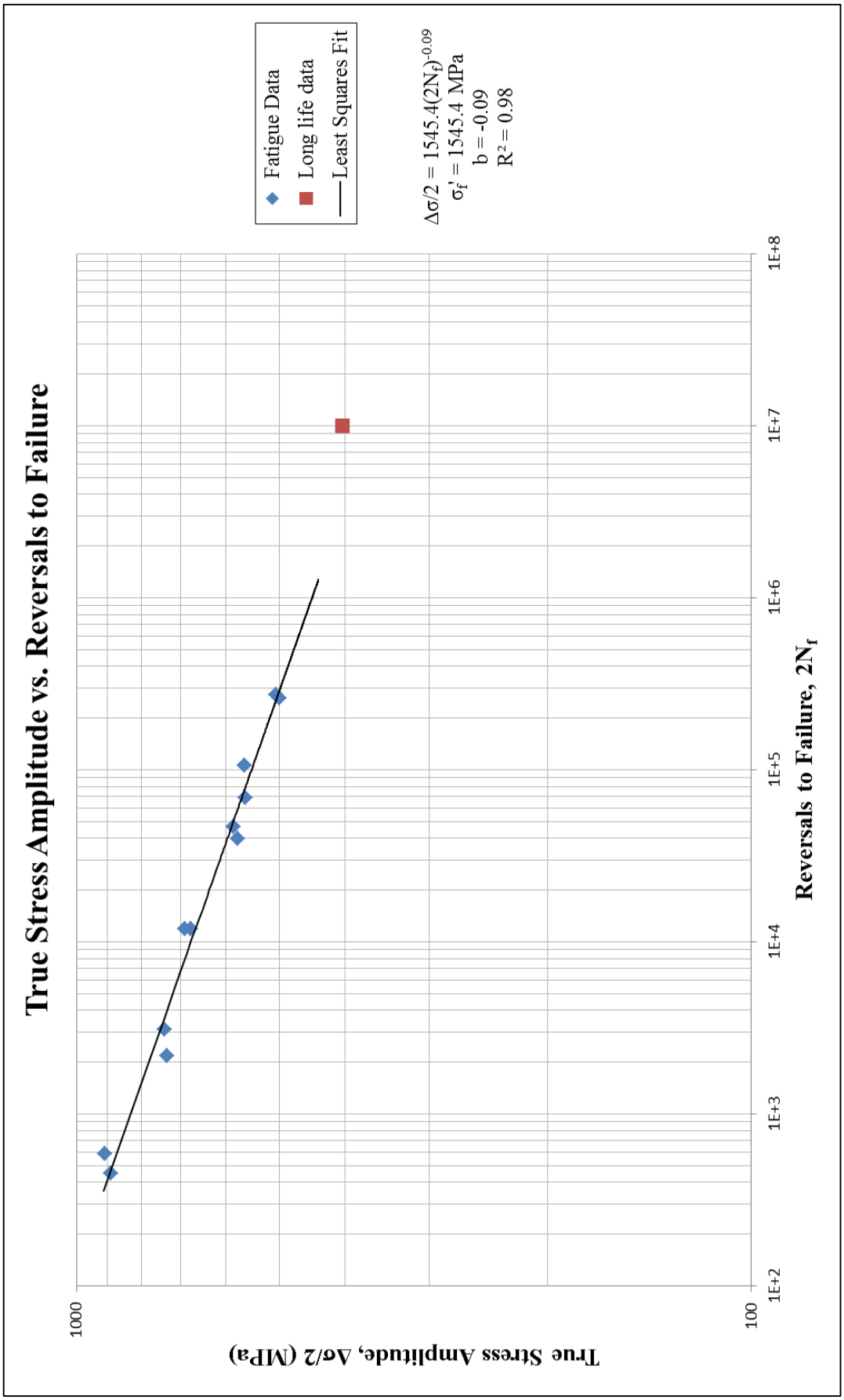


Figure 9: True stress amplitude versus reversals to failure

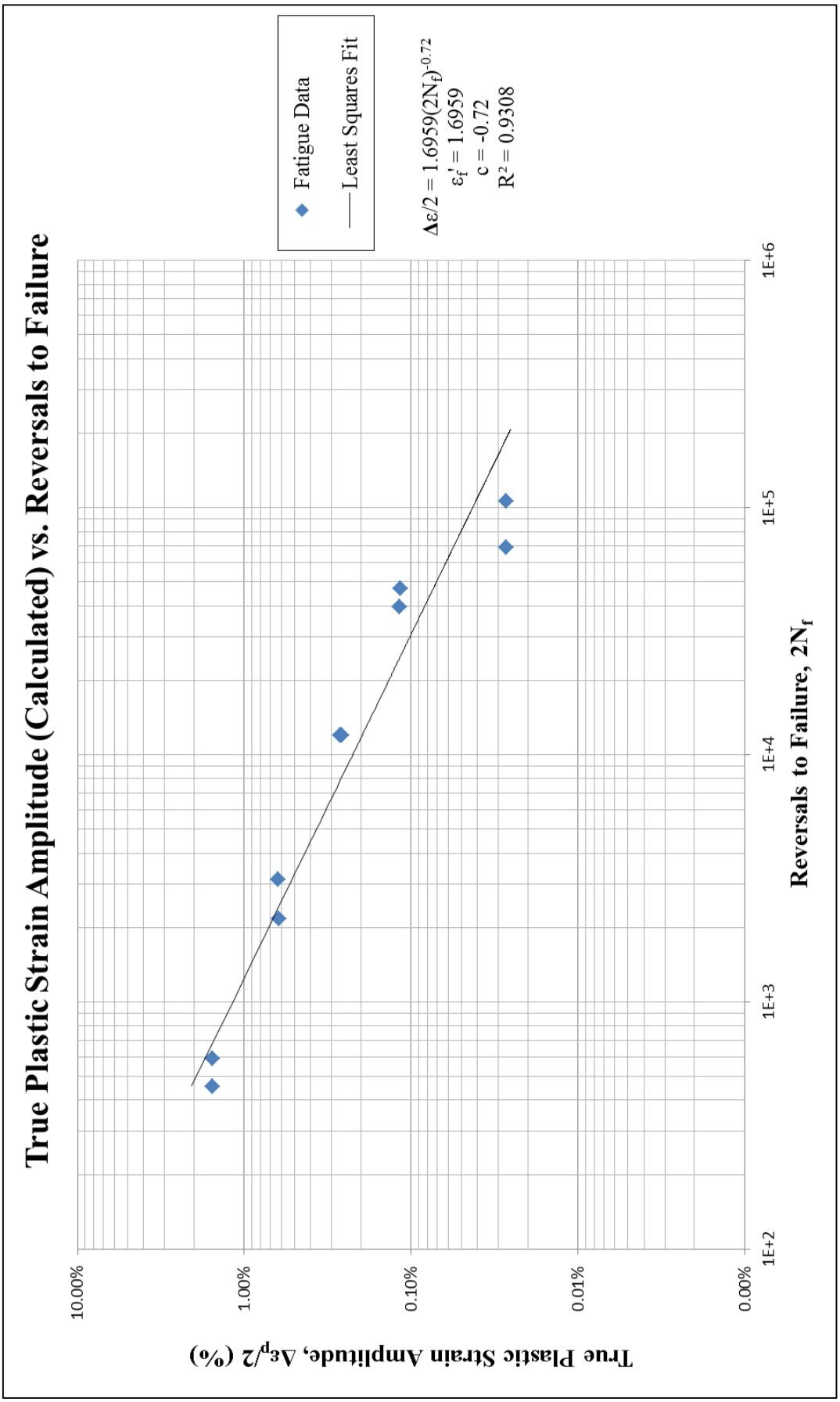


Figure 10: True plastic strain amplitude (calculated) versus reversals to failure

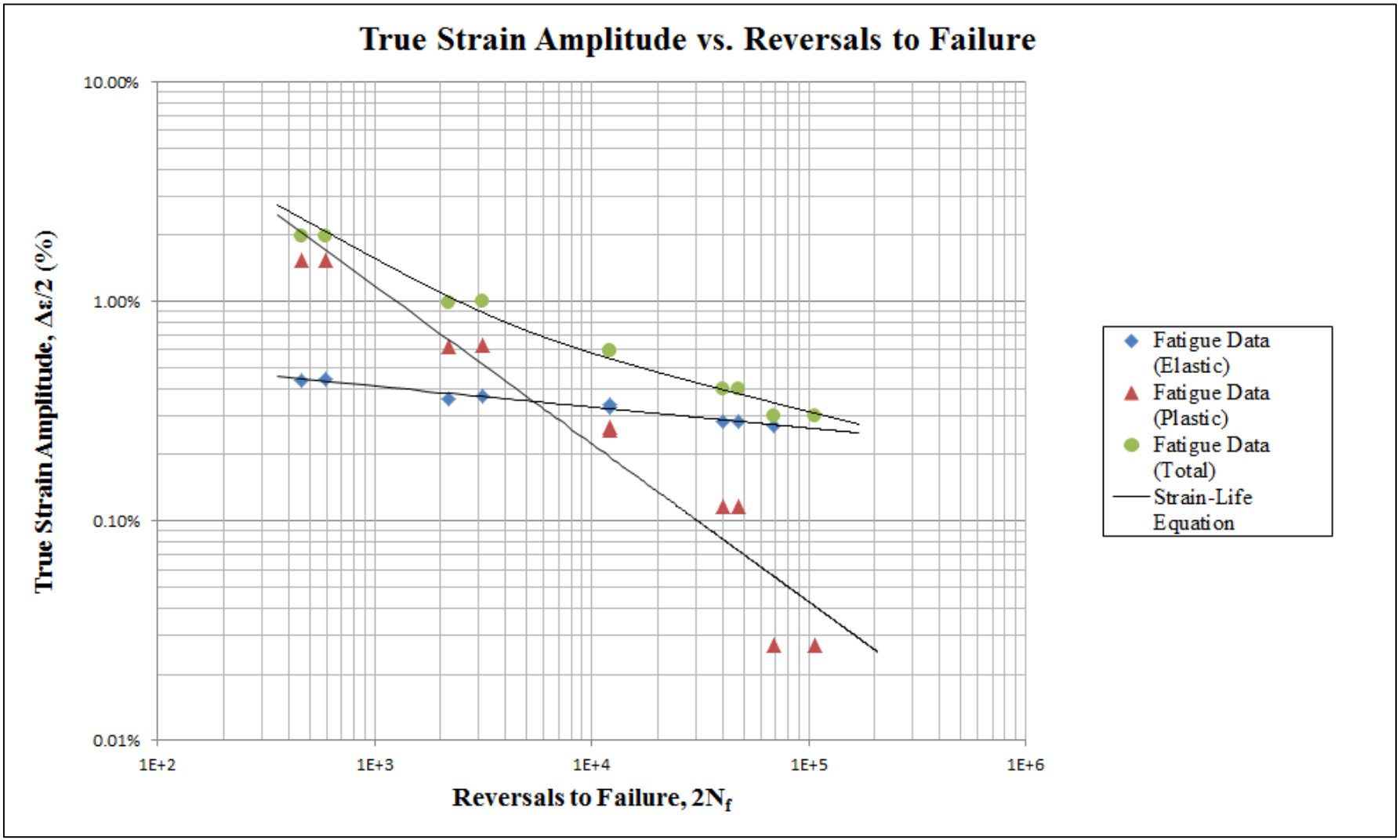


Figure 11: True strain amplitude versus reversals to failure

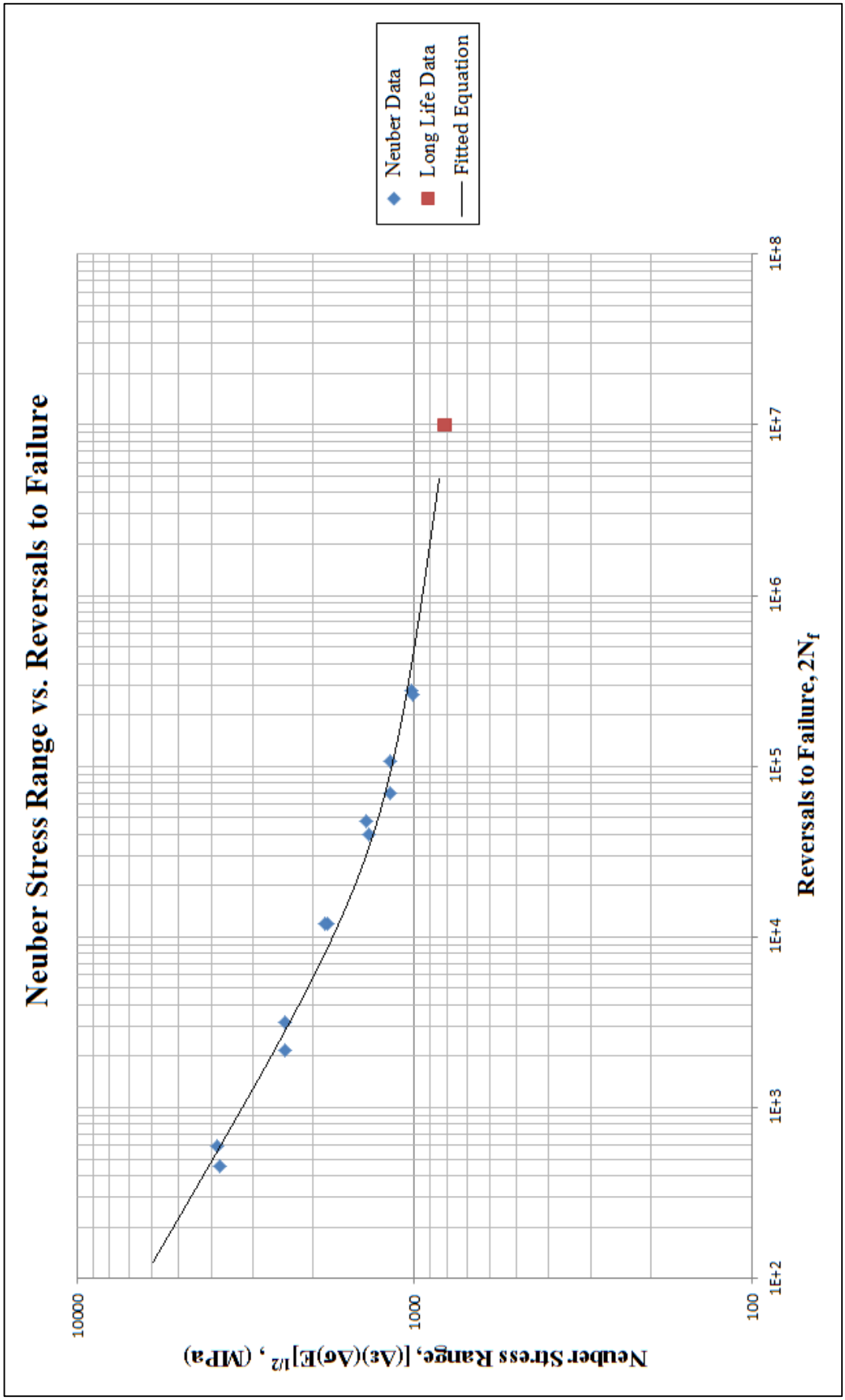


Figure 12: Neuber stress range versus reversals to failure

# REFERENCES

[1] ASTM Standard E606-92, "Standard Practice for Strain-Controlled Fatigue Testing", Annual Book of ASTM Standards, Vol. 03.01, 2004, pp. 593-606.

[2] ASTM Standard E83-02, "Standard Practice for Verification and Classification of Extensometers", Annual Book of ASTM Standards, Vol. 03.01, 2004, pp. 232-244.

[3] ASTM Standard E1012-99, "Standard Practice for Verification of Specimen Alignment Under Tensile Loading", Annual Book of ASTM Standards, Vol. 03.01, 2004, pp. 763-770.

[4] ASTM Standard E8-04, "Standard Test Methods for Tension Testing of Metallic Materials", Annual Book of ASTM Standards, Vol. 03.01, 2004, pp. 62-85.

[5] ASTM Standard E739-91, "Standard Practice for Statistical Analysis of Linear or Linearized Stress-Life (S-N) and Strain-Life (ε-N) Fatigue data", Annual Book of ASTM Standards, Vol. 03.01, 1995, pp. 670-676.

[6] ASTM Standard E646-00, "Standard Test Method for Tensile Strain-Hardening Exponents (n-values) of Metallic Sheet Materials", Annual Book of ASTM Standards, Vol. 03.01, 2004, pp. 619-626.

[7] Stephens R. I., Fatemi A., Stephens R.R. and Fuchs H. O., "*Metal Fatigue in Engineering*", Second edition, Wiley Interscience, 2000.

[8] Yung-Li Lee, Jwo Pan, Richard Hathaway, Mark Barkey, 2005, "*Fatigue Testing and Analysis*", Elsevier Inc.

# APPENDIX A

## Table A.1: Summary of monotonic tensile test results

| Specimen ID | $D_0$, mm | $D_f$, mm | R, mm | $L_0$, mm | $L_f$, mm | E, GPa | YS, MPa | $S_u$, MPa | K, MPa | n | %EL | %RA | $\varepsilon_f$ % | $\sigma_f$ MPa |
|---|---|---|---|---|---|---|---|---|---|---|---|---|---|---|
| 155_1 | 5.100 | 3.158 | 1.207 | 7.62 | 10.38 | 205.20 | 750.1 | 1014.8 | 1534.7 | 0.1106 | 36.2% | 61.9% | 96.4% | 1457.9 |
| 155_2 | 5.110 | 3.191 | 1.207 | 7.62 | 10.42 | 204.66 | 756.2 | 1007.1 | 1497.9 | 0.1076 | 36.7% | 61.0% | 94.2% | 1418.8 |
| AVG. | 5.105 | 3.175 | 1.207 | 7.62 | 10.40 | 204.93 | 753.2 | 1011.0 | 1516.3 | 0.1091 | 36.5% | 61.5% | 95.3% | 1438.3 |

## Table A.2: Summary of constant amplitude completely reversed fatigue test results

| Specimen ID | Applied Strain % | Test control mode | Test freq., Hz | E, GPa [e] | At midlife ($N_{50\%}$) | | | | | | | $(2N_f)_{10\%}$, [b] reversals | $(2N_f)_{50\%}$, [c] reversals | Failure location [d] |
|---|---|---|---|---|---|---|---|---|---|---|---|---|---|---|
| | | | | | E′, GPa | $\Delta\varepsilon/2$, % | $\Delta\varepsilon_p/2$, (calculated) % | $\Delta\varepsilon_p/2$, (measured) % | $\Delta\sigma/2$, MPa | $\sigma_m$, MPa | $2N_{50\%}$, [a] reversals | | | |
| 155_6 | ±2% | strain | 0.2 | 205.5 | 194.3 | 1.991% | 1.549% | 1.525% | 907.7 | -17.7 | 256 | 580 | 594 | IGL |
| 155_10 | ±2% | strain | 0.2 | 202.7 | 197.9 | 1.988% | 1.550% | 1.525% | 888.1 | -18.5 | 256 | 446 | 456 | IGL |
| 155_3 | ±1% | strain | 0.2 | 203.0 | 200.9 | 0.988% | 0.618% | 0.630% | 734.2 | -14.2 | 1,024 | 2,160 | 2,186 | IGL |
| 155_11 | ±1% | strain | 0.2 | 200.1 | 195.3 | 0.997% | 0.627% | 0.635% | 739.3 | -14.2 | 1,024 | 3,112 | 3,146 | IGL |
| 155_7 | ±0.6% | strain | 1.0 | 204.2 | 200.4 | 0.598% | 0.267% | 0.251% | 676.0 | -14.2 | 4,096 | 11,382 | 12,044 | IGL |
| 155_12 | ±0.6% | strain | 1.0 | 204.3 | 200.0 | 0.599% | 0.261% | 0.258% | 689.5 | -15.1 | 4,000 | 12,000 | 12,038 | IGL |
| 155_8 | ±0.4% | strain | 3.0 | 207.0 | 204.6 | 0.399% | 0.116% | 0.120% | 585.7 | -24.5 | 20,000 | 46,012 | 47,324 | IGL |
| 155_13 | ±0.4% | strain | 3.0 | 204.6 | 201.3 | 0.399% | 0.117% | 0.114% | 576.6 | -23.4 | 20,000 | 38,982 | 39,995 | IGL |
| 155_14 | ±0.3% | strain load | 1.0 10.0 | 206.9 | 206.6 | 0.300% | 0.027% | 0.027% | 563.5 | -20.6 | 60,000 | - | 107,068 | IGL |
| 155_9 | ±0.3% | load | 10.0 | 206.0 | 205.3 | 0.300% | 0.027% | 0.029% | 560.9 | -20.1 | 40,000 | - | 69,168 | IGL |
| 155_15 | ±0.25% | strain load | 1.0 20.0 | 205.9 | 207.2 | 0.250% | 0.004% | 0.005% | 505.7 | -5.5 | 131,072 | - | 277,104 | IGL |
| 155_18 | ±0.25% | load | 20.0 | 203.7 | 207.1 | 0.250% | 0.004% | 0.007% | 500.3 | -4.3 | 131,072 | - | 263,450 | IGL |
| 155_16 | ±0.2% | strain load | 1.0 25.0 | 202.5 | 202.6 | 0.200% | 0.000% | 0.000% | 403.3 | 0.0 | - | - | >10,000,000 | No Failure |
| 155_17 | ±0.2% | load | 25.0 | 206.3 | 206.3 | 0.200% | 0.000% | 0.000% | 403.4 | 0.0 | - | - | >10,000,000 | No Failure |

[a] $2N_{50\%}$ is defined as the midlife reversal;

[b] $(2N_f)_{10\%}$ is defined as reversal of 10% load drop;

[c] $(2N_f)_{50\%}$ is defined as reversal of 50% load drop or failure;

[d] IGL = Inside gage length

[e] E value was calculated from the first cycle.

## Table A.3: Measurement of Specimen Dimensions

| Specimen ID | Total Length (mm) | Grip Diameter (mm) | Grip Length* (mm) | Gage Diameter (mm) | Gage Length (mm) |
|---|---|---|---|---|---|
| 155_1 | 108.65 | 12.64 | 38.22/38.7 | 5.10 | 7.62 |
| 155_2 | 109.21 | 12.65 | 38.2/38.8 | 5.11 | 7.62 |
| 155_3 | 108.80 | 12.65 | 38.64 | 5.11 | 7.62 |
| 155_4 | 108.80 | 12.68 | 38.5 | 5.08 | 7.62 |
| 155_5 | 109.00 | 12.63 | 38.4/39.0 | 5.09 | 7.62 |
| 155_6 | 108.70 | 12.69 | 38.6/38.5 | 5.12 | 7.62 |
| 155_7 | 109.00 | 12.64 | 37.1/40.1 | 4.90 | 7.62 |
| 155_8 | 108.20 | 12.65 | 39.08/37.76 | 5.12 | 7.62 |
| 155_9 | 108.67 | 12.62 | 38.34/39.45 | 5.11 | 7.62 |
| 155_10 | 108.42 | 12.63 | 37.00/40.00 | 5.07 | 7.62 |
| 155_11 | 109.01 | 12.64 | 38.77 | 5.04 | 7.62 |
| 155_12 | 108.70 | 12.65 | 36.76/39.91 | 5.13 | 7.62 |
| 155_13 | 109.80 | 12.64 | 37.4/40.2 | 4.98 | 7.62 |
| 155_14 | 108.66 | 12.62 | 38.63 | 5.03 | 7.62 |
| 155_15 | 108.89 | 12.63 | 38.65/38.36 | 5.04 | 7.62 |
| 155_16 | 109.50 | 12.63 | 38.9 | 5.01 | 7.62 |
| 155_17 | 107.70 | 12.63 | 37.35/38.67 | 5.03 | 7.62 |
| 155_18 | 108.44 | 12.61 | 38.03/38.43 | 5.04 | 7.62 |

* For some of the specimens, the grip length of one side is different from the other side. Both dimensions are provided in the table.

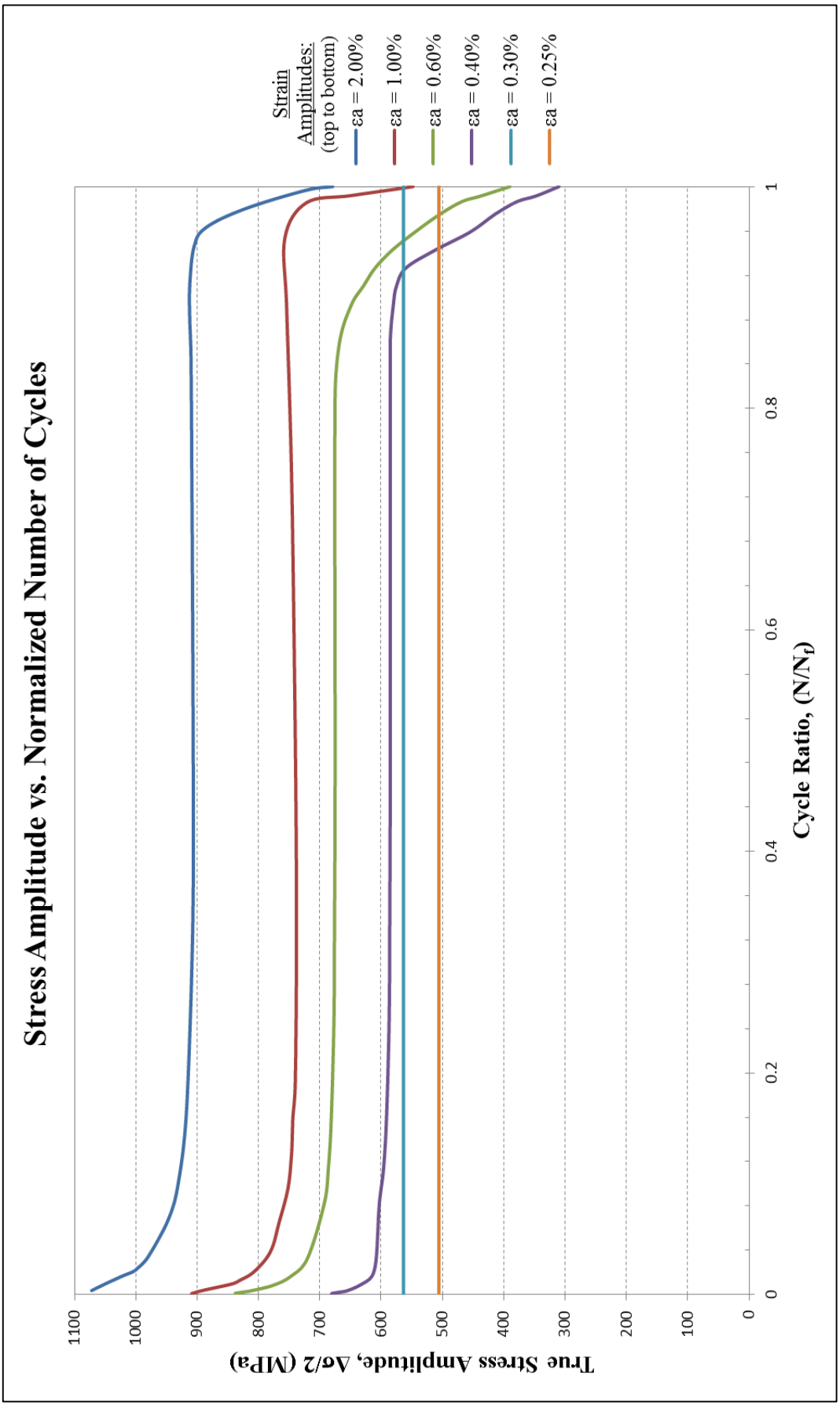


Figure A.1a: True stress amplitude versus normalized number of cycles

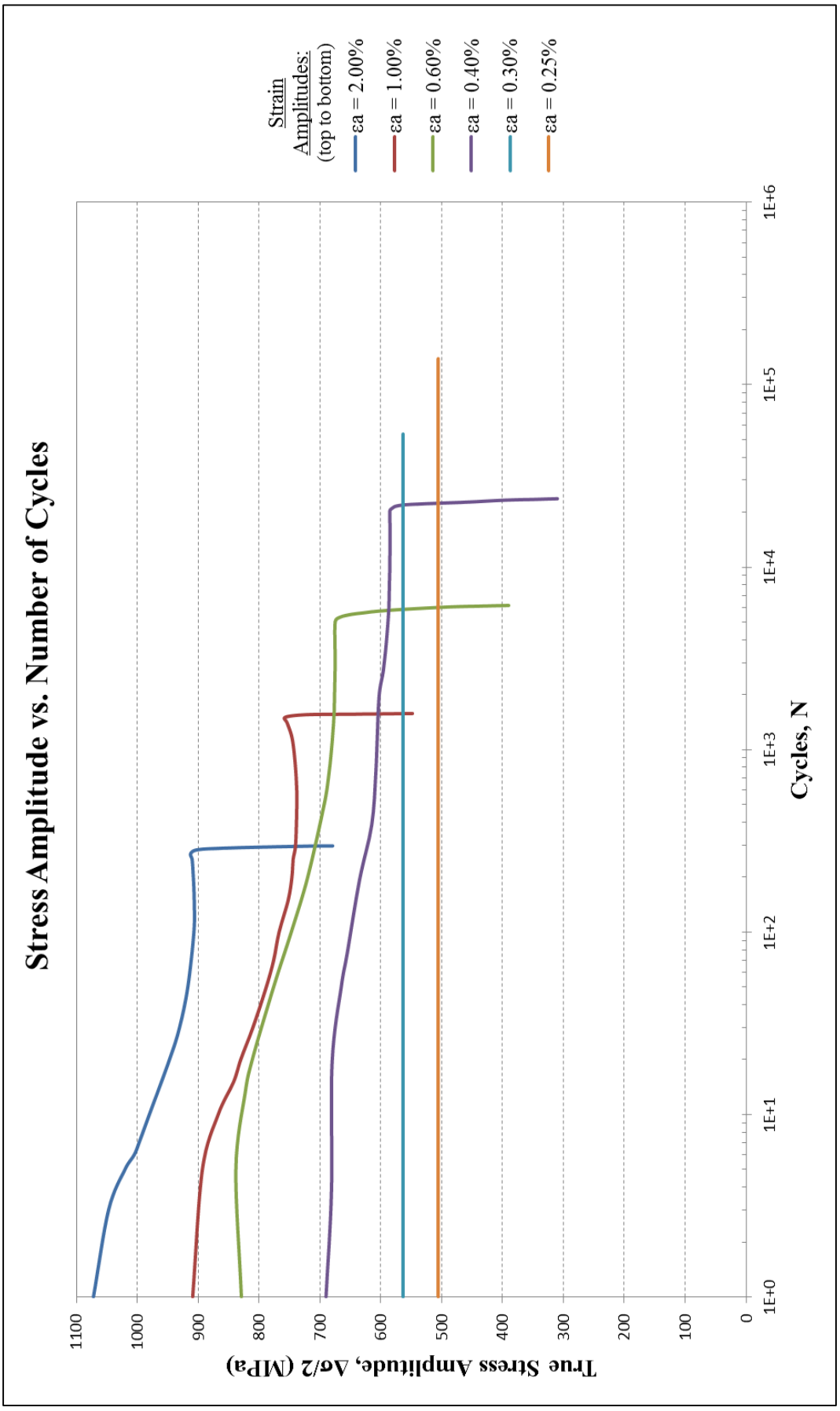


Figure A.1b: True stress amplitude versus number of cycles

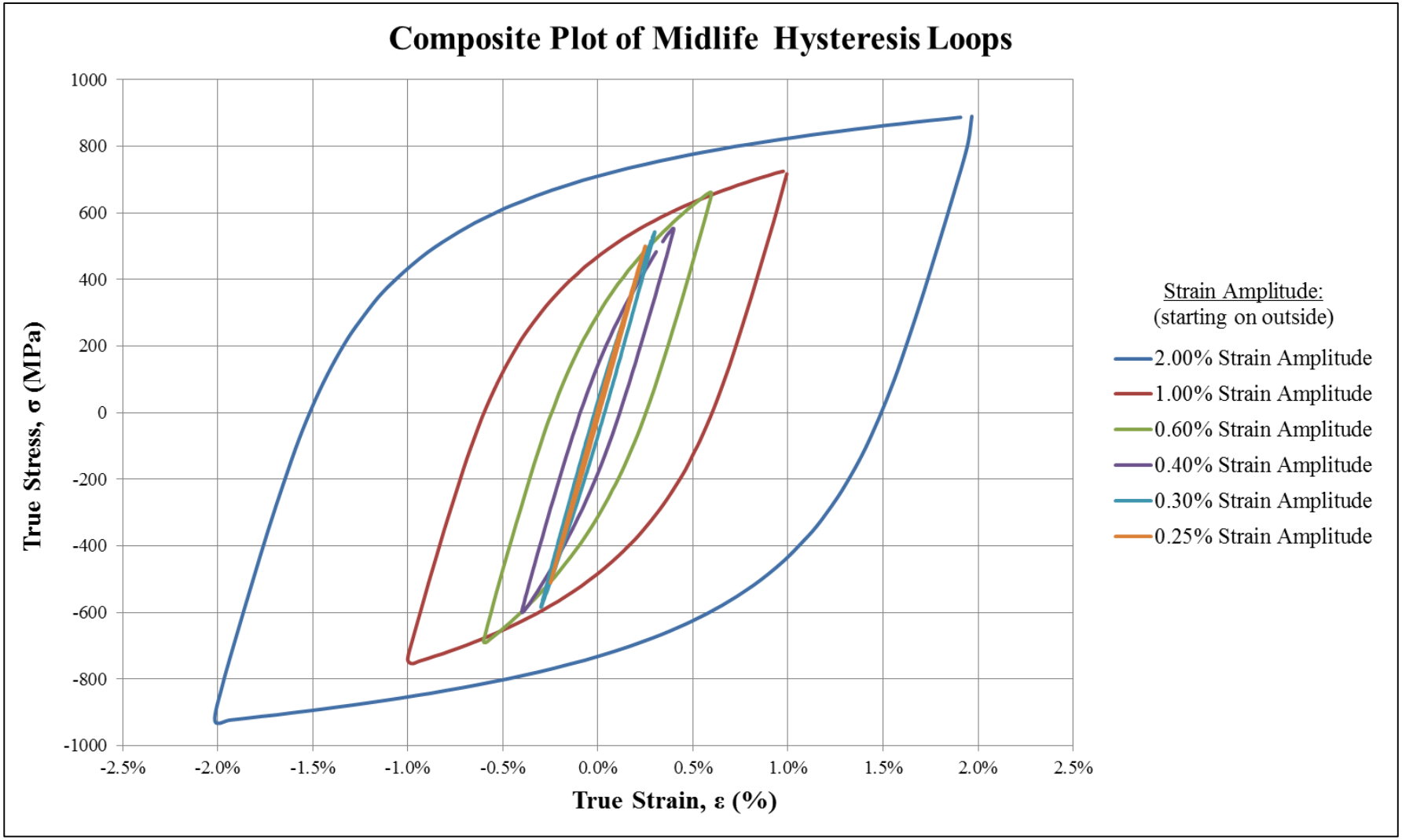


Figure A.2: Composite plot of midlife hysteresis loops

# APPENDIX B

## Rockwell Hardness Test

The Rockwell hardness number HR is determined by the difference in depth of penetration resulting from the application of an initial minor load followed by a larger major load.

A Rocky test machine was applied to get the Rockwell Hardness. Indenters include spherical and hardened steel balls and a conical diamond (Brale) indenter, which is used for the hardest materials. The 1/16-in. ball indenter was used for HRB scale, the diamond indenter was used for HRC scale. For the material of this project, we first use HRC to describle the hardness and found that it was not so hard (less than 20HRC). Then we change the indenter from diamond to 1/16-in. ball to get the HRB for accuracy. Here in this study, five specimens were applied for hardness testing, six different locations from each grip end surface were chosen for testing. The results are shown in Table B.1 and Table B.2.

Take the average value, the hardness for this material is 97.0 HRB (or 19.6 HRC).

**Table B.1: Rockwell Hardness (HRB)**

| Specimen ID | Data #1 | Data #2 | Data #3 | Data #4 | Data #5 | Data #6 | AVG |
|---|---|---|---|---|---|---|---|
| IT155_5 | 95.0 | 94.3 | 94.4 | 95.8 | 98.6 | 100.1 | **96.4** |
| IT155_7 | 94.4 | 95.0 | 96.3 | 94.0 | 97.3 | 95.7 | **95.5** |
| IT155_12 | 92.6 | 93.8 | 98.5 | 98.2 | 98.6 | 98.7 | **96.7** |
| IT155_15 | 100.0 | 100.1 | 100.3 | 101.4 | 100.3 | 98.9 | **100.2** |
| IT155_16 | 88.6 | 95.9 | 99.1 | 96.7 | 98.4 | 97.9 | **96.1** |

**Table B.2: Rockwell Hardness (HRC)**

| Specimen ID | Data #1 | Data #2 | Data #3 | Data #4 | Data #5 | Data #6 | AVG |
|---|---|---|---|---|---|---|---|
| IT155_5 | 17.0 | 16.2 | 16.3 | 18.5 | 21.6 | 23.0 | **18.8** |
| IT155_7 | 16.3 | 17.0 | 19.3 | 16.0 | 20.3 | 18.3 | **17.9** |
| IT155_12 | 14.1 | 15.8 | 21.5 | 21.2 | 21.6 | 21.7 | **19.3** |
| IT155_15 | 23.0 | 23.1 | 23.2 | 25.4 | 23.2 | 21.8 | **23.3** |
| IT155_16 | 9.6 | 18.9 | 22.1 | 19.7 | 21.4 | 20.9 | **18.8** |